

# Ion-induced effective surface diffusion in ion sputtering

Maxim A. Makeev and Albert-László Barabási<sup>a)</sup>

*Department of Physics, University of Notre Dame, Notre Dame, Indiana 46556*

(Received 10 July 1997; accepted for publication 11 September 1997)

Ion bombardment is known to enhance surface diffusion and affect the surface morphology. Here we demonstrate that preferential erosion during ion sputtering can lead to a physical phenomenon reminiscent of surface diffusion, what we call effective surface diffusion (ESD), that does not imply mass transport along the surface and is independent of the temperature. We calculate the ion-induced ESD constant and its dependence on the ion energy, flux and angle of incidence, showing that sputtering can both enhance and suppress surface diffusion. The influence of ion-induced ESD on ripple formation and roughening of ion-sputtered surfaces is discussed and summarized in a morphological phase diagram. © 1997 American Institute of Physics. [S0003-6951(97)02245-6]

Sputtering, the removal of atoms from the surface of solids through the impact of energetic particles (ions), is an important thin film processing technique.<sup>1</sup> Consequently, much attention has been focused on the measurement and calculation of the sputtering yield and of the velocity and angular distribution of the sputtered particles. However, for many applications an equally important phenomenon, ion-induced surface diffusion,<sup>3-8</sup> has eluded sufficient understanding so far. In the absence of ion bombardment surface diffusion is thermally activated and characterized by the diffusion constant  $D_T = D_0 \exp[-E_d/k_B T]$ , such that the evolution of the surface height  $h(x, y, t)$  is described by the continuum equation  $\partial h / \partial t = -D_T \nabla^4 h$ .<sup>2</sup> Here  $E_d$  is the activation energy for surface diffusion of the adatoms and  $T$  is the substrate temperature. The most common effect of ions on surface diffusion is related to direct transfer of the energy and momentum to the surface atoms by ion-atom collisions, changing the diffusion probability of an atom to diffuse from  $P \sim \exp(-E_d/k_B T)$  to  $P \sim \exp[-(E_d - E_i)/k_B T]$ , where  $E_i$  is the energy transferred from the ion to the surface atom. However, a different mechanism appears to take place for higher energies, when the substrate is eroded by ion-bombardment: in this case the effective diffusion is independent of temperature. For example, MacLaren *et al.*<sup>5</sup> bombarded GaAs with 17 keV Cs<sup>+</sup> in the temperature range from -50 to 200 °C, observing the development of a ripple structure on the surface with a wavelength proportional to the square root of the diffusion constant. When decreasing the temperature, the ripple spacing (wavelength) did not decrease exponentially to zero with the inverse temperature, but at 55 °C it stabilized at a constant value, providing direct evidence for a temperature independent ion-induced surface diffusion constant. Similar effects were observed for SiO<sub>2</sub> bombarded by 5 keV atoms, and strong evidence for this process is provided by the recent numerical simulations by Koponen *et al.*,<sup>9</sup> who observed ripple formation even when surface diffusion was absent in the model. Although the effect of the ions on surface diffusion is well documented experimentally and numerically, there is no theory that would quantify it. In this letter we demonstrate the existence of a

new mechanism for ion-induced diffusion, showing that sputtering can lead to preferential erosion that appears as surface diffusion, even though no actual mass transport along the surface takes place in the system. To distinguish it from ordinary surface diffusion, in the following we refer to the ion-induced component,  $D^I$ , as effective surface diffusion (ESD) constant. We calculate analytically the ESD constant and its dependence on the ion energy, flux, angle of incidence, and penetration depth. We find that there exists a parameter range when ion bombardment generates a negative ESD constant, leading to morphological instabilities along the surface, affecting the surface roughness and the ripple structure.

Ion-beam sputtering is determined by atomic processes taking place within a finite penetration depth inside the bombarded material. A convenient picture of the ion bombardment process is shown in Fig. 1. The ions penetrate a distance  $a$  inside the bulk of material before they completely spread out their kinetic energy with some assumed spatial distribution. An ion releasing its energy at point  $P$  in the solid contributes energy to the surface point  $O$ , that may induce the atoms in  $O$  to break their bonds and leave the surface or diffuse along it.

Following,<sup>10,11</sup> we consider that the average energy deposited at point  $O$  due to the ion arriving at  $P$  follows the Gaussian distribution<sup>12</sup>

$$E(\mathbf{r}') = \frac{\epsilon}{(2\pi)^{3/2} \sigma \mu^2} \exp\left\{-\frac{z'^2}{2\sigma^2} - \frac{x'^2 + y'^2}{2\mu^2}\right\}. \quad (1)$$

In Eq. (1)  $z'$  is the distance measured along the ion trajectory,  $x', y'$  are measured in the plane perpendicular to it;  $\epsilon$  denotes the kinetic energy of the ion and  $\sigma$  and  $\mu$  are the widths of the distribution in directions parallel and perpendicular to the incoming beam, respectively. However, the sample is subject to a uniform flux  $J$  of bombarding ions. A large number of ions penetrate the solid at different points simultaneously, and the velocity of erosion at  $O$  depends on the total power  $\mathcal{E}_O$  contributed by all the ions deposited within the range  $\mathcal{R}$  of the distribution [Eq. (1)], such that

$$v = p \int_{\mathcal{R}} d\mathbf{r} \Phi(\mathbf{r}) E(\mathbf{r}), \quad (2)$$

<sup>a)</sup>Electronic mail: alb@nd.edu

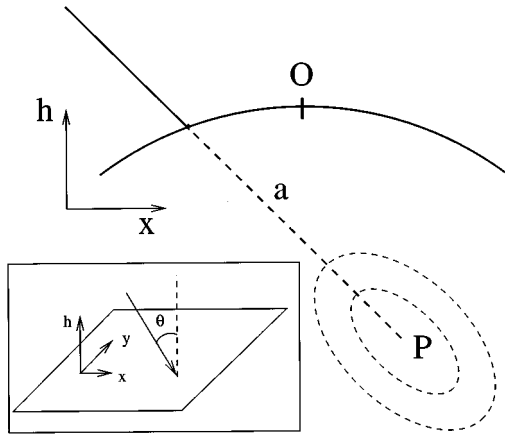


FIG. 1. Following a straight trajectory (solid line) the ion penetrates an average distance  $a$  inside the solid (dotted line) after which it completely spreads out its kinetic energy. The energy decreases with the distance from  $P$ , the dotted curves indicating schematically the equal energy contours. The energy released at point  $P$  contributes to erosion at  $O$ . The inset shows the laboratory coordinate frame: the ion beam forms an angle  $\theta$  with the normal to the average surface orientation,  $z$ , and the in-plane direction  $x$  is chosen along the projection of the ion beam.

where  $\Phi(\mathbf{r})$  corrects for the local slope dependence of the uniform flux  $J$  and  $p$  is a proportionality constant between power deposition and the erosion rate.<sup>10</sup> The calculation of  $v$  involves the following assumptions (for more details see Refs. 11 and 12): (a) In the laboratory coordinate frame  $(x, y, z)$  the surface can be described by a single valued height function  $h(x, y, t)$ , measured from an initial flat configuration which lies in the  $(x, y)$  plane (see Fig. 1); (b) the angle between the ion beam direction and the local normal to the surface is a function of the angle of incidence  $\theta$  and the values of the local slopes  $\partial_x h$  and  $\partial_y h$ , and can be expanded in powers of the latter. Under these conditions, we can expand Eq. (2), obtaining the equation of motion

$$\begin{aligned} \frac{\partial h}{\partial t} = & -v_0 + \gamma \frac{\partial h}{\partial x} + \nu_x \frac{\partial^2 h}{\partial x^2} + \nu_y \frac{\partial^2 h}{\partial y^2} + \frac{\lambda_x}{2} \left( \frac{\partial h}{\partial x} \right)^2 \\ & + \frac{\lambda_y}{2} \left( \frac{\partial h}{\partial y} \right)^2 - D_x^I \frac{\partial^4 h}{\partial x^4} - D_y^I \frac{\partial^4 h}{\partial y^4}. \end{aligned} \quad (3)$$

Here  $v_0$  is the erosion rate, the second term accounts for uniform motion of the surface features along the  $x$  direction,<sup>10,12</sup>  $\nu_x$  and  $\nu_y$  represent ion-induced surface tension terms,  $\lambda_x$  and  $\lambda_y$  characterize the slope dependence of the erosion rate, while  $D_x^I$  and  $D_y^I$  are the ion-induced ESD coefficients.

From Eq. (2) we can calculate the expressions for these coefficients in terms of the physical parameters which characterize the sputtering process. The coefficients  $\nu_x$  and  $\nu_y$  were first calculated by Bradley and Harper,<sup>11</sup> while the non-linear expansion was performed in,<sup>12</sup> providing  $\lambda_x$  and  $\lambda_y$ . A fourth order expansion is used to obtain the ion-induced ESD constants  $D_x^I$  and  $D_y^I$ . While the calculations were performed for arbitrary  $\sigma$  and  $\mu$ , to simplify the discussion we restrict ourselves to the symmetric case  $\sigma = \mu$ . Using  $F \equiv (\epsilon J p / \sqrt{2\pi}) \exp(-a_\sigma^2/2 + a_\sigma^2 s^2/2)$ ,  $s \equiv \sin \theta$ ,  $c \equiv \cos \theta$ , and  $a_\sigma \equiv a/\sigma$ , we find for the ESD constants

$$D_x^I = \frac{F a^2}{24 a_\sigma} \{ a_\sigma^4 s^4 c^2 + a_\sigma^2 (6c^2 s^2 - 4s^4) + 3c^2 - 12s^2 \}, \quad (4)$$

$$D_y^I = \frac{F a^2}{24 a_\sigma} 3c^2. \quad (5)$$

The consequences of Eqs. (4) and (5) can be summarized as follows:

(a) It is important to note that Eqs. (4) and (5) do not imply that there is mass transport along the surface. The effective surface diffusion terms [Eqs. (4) and (5)] are generated by preferential erosion of the substrate, i.e., certain parts of the substrate are eroded faster than other parts, depending on the local surface morphology. If the system is viewed from the coordinate frame moving together with average height [which in our formalism is done by separating the constant erosion rate  $v_0$  in Eq. (3)] this preferential erosion appears as a reorganization of the surface, corresponding to a surface diffusionlike mechanism. For this to happen, actual atomic diffusion is not required.

(b) Independent of sign of the angle of incidence  $D_y^I$  is positive while the sign of the  $D_x^I$  depends on both  $\theta$  and  $a_\sigma$ . Thus, while for  $\theta=0$  the ion bombardment enhances the surface diffusion ( $D_x^I > 0$ ), for large  $\theta$  it can suppress the surface diffusion (see below).

(c) It is a standard experimental practice to report the magnitude of the ion-enhanced diffusion using an effective temperature  $T^{\text{eff}}$ , at which the substrate needs to be heated to obtain the same mobility as with ion bombardment.<sup>7,8</sup> We can calculate  $T^{\text{eff}}$  using the relation  $D^I + D_0 \exp(-E_a/k_B T) = D_0 \exp(-E_a/k_B T^{\text{eff}})$ . The anisotropic ESD constant translates into an anisotropic  $T^{\text{eff}}$ , i.e., we have  $T_x^{\text{eff}} \neq T_y^{\text{eff}}$ .

(d) The results [Eqs. (4) and (5)] are based on Sigmund's theory of sputtering<sup>10</sup> that describes sputtering in the linear cascade regime. The energy range when this approach is applicable lies between 0.5 keV and 1 meV, the precise lower and upper limits being material dependent.

(e) Finally, we estimate the ESD coefficient. Taking<sup>11</sup>  $p = 10^{-31} \text{ cm}^4/\text{eV}$ ,  $a = 100 \text{ \AA}$ , typical flux  $J = 10^{15} \text{ ions/cm}^2 \text{ s}$  we obtain  $D^I = 10^{-24} \text{ cm}^4/\text{s}$ . Bradley and Harper<sup>11</sup> estimated the value of the thermally activated diffusion coefficient for the same material and ion conditions, obtaining  $D_T = 10^{-22} \text{ cm}^4/\text{s}$  for  $T = 700 \text{ }^\circ\text{C}$ . Thus, since  $D_T$  decreases exponentially with temperature,  $D^I$  can be significant at low temperatures, in some cases being comparable or larger than the thermal diffusion constant (note that McLaren *et al.*<sup>5</sup> observed the temperature independent ripple wavelength in the range of 20–60  $^\circ\text{C}$ ).

*Ripple formation*—The origin of the ripple formation during ion sputtering is an ion-induced instability:<sup>13</sup> valleys are eroded faster than crests, expressed by negative  $\nu_x$  and  $\nu_y$  coefficients in Eq. (3).<sup>11</sup> At short wavelength this instability is balanced by surface diffusion. A linear stability analysis predicts that the observable ripple wavelength is  $l = 2\pi \sqrt{D/|\nu|}$ , where  $\nu$  is the largest in absolute value of the negative surface tension coefficients. Accordingly, the wave vector of the ripples is parallel to the  $x$  axis for small  $\theta$  and perpendicular to it for large  $\theta$ .<sup>11</sup> The large length scale behavior is described by the noisy anisotropic Kuramoto–

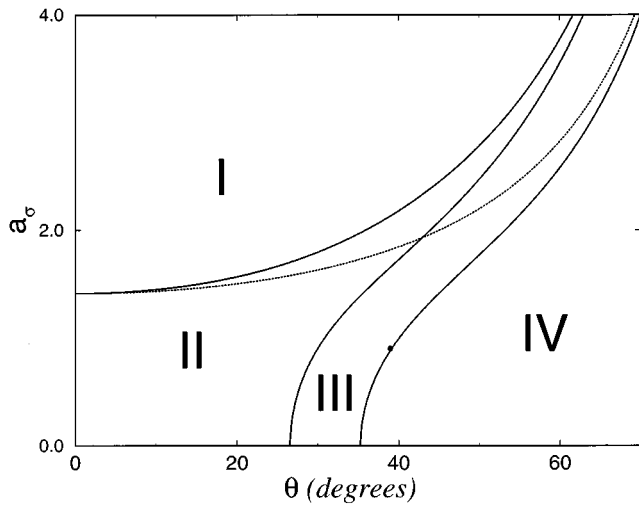


FIG. 2. Phase diagram for the isotropic case  $\sigma = \mu = 1$ . Region I:  $\nu_x < 0$ ,  $\nu_y < 0$ ,  $D_x^I > 0$ ,  $D_y^I > 0$ , and  $l_x > l_y$ ; region II:  $\nu_x < 0$ ,  $\nu_y < 0$ ,  $D_x^I > 0$ ,  $D_y^I > 0$ , and  $l_x < l_y$ ; region III:  $\nu_x < 0$ ,  $\nu_y < 0$ ,  $D_x^I < 0$ , and  $D_y^I > 0$ ; region IV:  $\nu_x > 0$ ,  $\nu_y < 0$ ,  $D_x^I < 0$ , and  $D_y^I > 0$ . Note that the phase diagram is independent of the precise values of  $J$ ,  $p$ , while the  $\epsilon$  dependence is contained in  $a_\sigma$ .

Sivashinsky (KS) equation,<sup>12,14</sup> leading to roughening<sup>15</sup> or the development of coarsening ripple domains.<sup>16</sup>

At finite temperatures the total diffusion constant is given by  $D = D^I + D_T$ . As  $T$  decreases, there is critical temperature,  $T_c$ , at which  $D^I = D_T$ , so that for  $T < T_c$  the diffusion is dominated by its ion-induced component, which is independent of temperature, in agreement with the experimental results of MacLaren *et al.*,<sup>5</sup> who observe that  $l$  is constant for  $T < T_c = 55$  °C. Numerical support for this effect was provided by the simulations of Koponen *et al.*,<sup>9</sup> who find that ripples develop even in the absence of surface diffusion.

**Morphological phase diagram**—The detailed morphological phase diagram is rather complex if the diffusion is not thermally activated, but ion-induced. At low temperatures, when  $D_T$  is negligible compared to  $D^I$ , the ripple wavelengths are  $l_x^I = 2\pi\sqrt{D_x^I/|\nu_x|}$  and  $l_y^I = 2\pi\sqrt{D_y^I/|\nu_y|}$ . In the following we discuss the dependence of the surface morphologies on the experimental parameters  $\theta$  and  $a_\sigma$ , based on the phase diagram shown in Fig. 2.

**Region I**—The surface tensions,  $\nu_x$  and  $\nu_y$ , are negative while  $D_x$  and  $D_y$  are positive, consequently we have a superimposed ripple structure along the  $x$  and  $y$  directions. The experimentally observed ripple wavelength is the smallest of the two, and since  $l_x^I > l_y^I$ , the ripple wave vector is oriented along the  $y$  direction. The lower boundary of this region separating it from region II is given by the solution of the  $l_x^I = l_y^I$  equation.

**Region II**—Here the ripple wave vector is oriented along the  $x$  direction, since  $l_x^I < l_y^I$ . This region is bounded below by the  $D_x^I = 0$  line. At large length scales in regions I and II one expects kinetic roughening described by the Kardar–Parisi–Zhang (KPZ) equation.<sup>12,17,18</sup>

**Region III**—In this region  $D_x^I$  is negative, while the signs of all other coefficients are the same as in regions I and II. Since both surface tension and surface diffusion are destabilizing along  $x$ , every mode is unstable and one expects that

the KPZ nonlinearity cannot turn on the KS stabilization,<sup>12</sup> the system being unstable at large length scales as well. This instability is expected to lead to exponential roughening. The lower boundary of this region is given by the  $\nu_x = 0$  line.

**Region IV**—Here we have  $\nu_x > 0$ ,  $\nu_y < 0$ ,  $D_{xx}^I < 0$ , and  $D_{yy}^I > 0$ , i.e., one expects the surface to be periodically modulated in the  $y$  direction, leading to a ripple structure oriented along the  $x$  direction. In the  $x$  direction we have a reversal of the instability: the short length scale instability generated by the negative  $D_x^I$  is stabilized by the positive surface tension  $\nu_x$ . Thus, there is no ripple structure along the  $y$  direction. Regarding the large length scale behavior, along the  $x$  direction the surface diffusion term is irrelevant compared to the surface tension, thus one expects KPZ scaling. However, along the  $y$  direction the KS mechanism is expected to act, renormalizing the negative  $\nu_y$  to positive values for length scales larger than  $l_y^I$ , leading to a large wavelength KPZ behavior.

The authors would like to acknowledge discussions and comments by R. Cuerno. This research was partially supported by the University of Notre Dame Faculty Research Program.

<sup>1</sup> *Sputtering by Particle Bombardment*, edited by R. Behrisch (Springer, Heidelberg, 1981, 1983), Vols. I–III.

<sup>2</sup> C. Herring, *J. Appl. Phys.* **21**, 301 (1950); W. W. Mullins, *ibid.* **28**, 333 (1957); in the context of stochastic models see D. E. Wolf and J. Villain, *Europhys. Lett.* **13**, 389 (1990); S. Das Sarma and P. I. Tamborenea, *Phys. Rev. Lett.* **66**, 325 (1991).

<sup>3</sup> V. O. Babaev, Ju. V. Bukov, and M. B. Guseva, *Thin Solid Films* **38**, 1 (1976).

<sup>4</sup> M. Marinov, *Thin Solid Films* **46**, 267 (1977).

<sup>5</sup> S. W. MacLaren, J. E. Baker, N. L. Finnegan, and C. M. Loxton, *J. Vac. Sci. Technol. A* **10**, 468 (1992).

<sup>6</sup> S. A. Barnett, H. F. Winters, and J. E. Greene, *Surf. Sci.* **181**, 596 (1987); Zh. I. Dranov and I. M. Mikhailovskii, *Sov. Phys. Solid State* **12**, 104 (1970); E. Chason, P. Bedrossian, K. M. Horn, J. Y. Tsao, and S. T. Picraux, *Appl. Phys. Lett.* **57**, 1793 (1990); E. Kay and S. M. Rossnagel, ‘‘Handbook of ion beam processing technology,’’ in *Sputtering by Particle Bombardment*, edited by R. Behrisch (Springer, Heidelberg, 1981, 1983).

<sup>7</sup> J. Y. Cavaille and M. Drechsler, *Surf. Sci.* **75**, 342 (1978).

<sup>8</sup> S. M. Rossnagel, R. S. Robinson, and H. R. Kaufman, *Surf. Sci.* **123**, 89 (1982).

<sup>9</sup> I. Koponen, M. Hautala, and O.-P. Sievanen, *Phys. Rev. Lett.* **78**, 2612 (1997).

<sup>10</sup> P. Sigmund, *Phys. Rev.* **184**, 383 (1969); *J. Mater. Sci.* **8**, 1545 (1973).

<sup>11</sup> R. M. Bradley and J. M. E. Harper, *J. Vac. Sci. Technol. A* **6**, 2390 (1988).

<sup>12</sup> R. Cuerno and A.-L. Barabási, *Phys. Rev. Lett.* **74**, 4746 (1995).

<sup>13</sup> E. Chason, T. M. Mayer, B. K. Kellerman, D. N. McIlroy, and A. J. Howard, *Phys. Rev. Lett.* **72**, 3040 (1994); T. M. Mayer, E. Chason, and A. J. Howard, *J. Appl. Phys.* **76**, 1633 (1994); G. Carter, B. Navinšek, and J. L. Whitton, see Ref. 1, Vol. II, p. 231.

<sup>14</sup> Y. Kuramoto and T. Tsuzuki, *Prog. Theor. Phys.* **55**, 356 (1977); G. I. Sivashinsky, *Acta Astron.* **6**, 569 (1979).

<sup>15</sup> E. A. Eklund, R. Bruinsma, and J. Rudnick, *Phys. Rev. Lett.* **67**, 1759 (1991); *Surf. Sci.* **285**, 157 (1993); J. Krim, I. Heyvaert, C. Van Haesendonck, and Y. Bruynseraede, *Phys. Rev. Lett.* **70**, 57 (1993); H.-N. Yang, G.-C. Wang, and T.-M. Lu, *Phys. Rev. B* **50**, 7635 (1994).

<sup>16</sup> M. Rost and J. Krug, *Phys. Rev. Lett.* **75**, 3894 (1995).

<sup>17</sup> M. Kardar, G. Parisi, and Y.-C. Zhang, *Phys. Rev. Lett.* **56**, 889 (1986).

<sup>18</sup> *Dynamics of Fractal Surfaces*, edited by F. Family and T. Vicsek (World Scientific, Singapore, 1991); W. M. Tong and R. S. Williams, *Annu. Rev. Phys. Chem.* **45**, 405 (1994); A.-L. Barabási and H. E. Stanley, *Fractal Concepts in Surface Growth* (Cambridge University Press, Cambridge, 1995).